Evolution of palladium sulfide phases during thermal treatments and consequences for acetylene hydrogenation

Yanan Liu,[1,2] Alan J. McCue,[2] Junting Feng,[1]* Shaoliang Guan,[3] Dianqing Li[1] and James A. Anderson[2]*

[1] State Key Laboratory of Chemical Engineering, Beijing University of Chemical Technology, Beijing 100029, China.

[2] Surface Chemistry and Catalysis Group, Materials and Chemical Engineering, Department of Engineering, University of Aberdeen, Aberdeen, UK, AB24 3UE.

[3] Cardiff Catalysis Institute, School of Chemistry, Cardiff University, Cardiff, UK, CF10 3AT

Tel: +44 1224 272838, Email: fengjt@mail.buct.edu.cn; j.anderson@abdn.ac.uk

Abstract

Unsupported, bulk phase palladium sulfide has been studied for the selective hydrogenation of acetylene. The sample underwent significant change during thermal pretreatments, the extent of which depends on temperature. Exposure to hydrogen at temperatures of 150°C or above results in the loss of sulfur from the sample, primarily as hydrogen sulfide. As sulfur is lost, the sample is progressively transformed from a sulfur rich phase (PdS) to a sulfur lean phase (Pd_4S) *via* an intermediate phase ($Pd_{16}S_7$). Reduction at 250°C produces a material, which contains simultaneously these three phases mentioned above with some Pd_4S phase is located at the surface, whereas reduction at 350°C results in a largely pure Pd_4S phase. Thermal treatments which produce a Pd_4S surface display excellent catalytic properties. At complete acetylene conversion at 250°C, ethylene selectivites of 82.8% and 90.0% were obtained under non-competitive and competitive conditions, respectively. Beneficial catalytic properties arise from the uniformity of Pd sites due to the crystal structure of Pd_4S along with electronic influences on the adsorption/desorption processes arising from sulfur neighbours. No indications of deactivation or obvious deposition of carbon were observed over Pd_4S sample after 50 h on stream.

Keywords

Acetylene, ethylene, selective hydrogenation, palladium sulphide

Introduction

A significant proportion of ethylene used for polymerisation is derived from naphtha cracking. This process results in an ethylene stream contaminated with 0.5-2% of acetylene, which can poison the polymerisation catalysts.[1,2,3] To remove the impurity to an acceptable level (<5 ppm), selective hydrogenation of acetylene is widely employed as it generates additional ethylene and therefore increases profitability. [4] Thermodynamics makes this process viable [5] when both acetylene and ethylene are present, since the adsorption energy of acetylene is generally greater on most surfaces than that of ethylene contributing to preferential adsorption. However, when acetylene concentration is low (i.e., near the 5 ppm requirement), ethylene is free to adsorb resulting in over-hydrogenation to ethane, thereby decreasing process efficiency and profitability. Furthermore, acetylene based oligomerisation results in the formation of green oil (C_xH_y), which accumulates on the catalyst surface leading to gradual deactivation. [1] The extent to which deactivation occurs depends on plant design. A 'front-end' type reactor is situated upstream of the demethaniser, and the feed gas contains a large excess of hydrogen. In contrast, a 'back-end' type reactor uses a purified gas feed to which a near stoichiometric amount of hydrogen can be added. Deactivation is relatively rapid in hydrogen lean conditions resulting in the need to regenerate more frequently. [6] Despite this limitation, back-end type reactors are the most common plant configuration. Industrial catalysts for this process generally contain Pd as the active component but require the use of Ag as a structural modifier [7] with CO often used to compete with ethylene for adsorption sites to supress over-hydrogenation. [2] Pd-based catalysts generally demonstrate high activity but limited selectivity in this reaction due to hydride/carbide formation [8,9,10,11,12,13] with calculations suggesting that the barrier for ethylene desorption is higher than that for over-hydrogenation. [14]

A common approach to improve ethylene selectivity over Pd nanocatalysts is to alloy with a second metal such as Ag [15,16,17], Au[18,19], Cu[20,21,22,23,24], Ni[25], and Zn[26], which dilutes Pd and reduces the ensemble size, and thus inhibits formation of the β-PdH phase. [11] In recent literature, the idea of 'Pd active site isolation' has become popular and typically contributes to enhanced alkene selectivity. [27] Well defined intermetallic PdM compounds (M=Ga, In, Cu) fall within this category and favour the enhancement of selectivity but at the expense of activity. [28,29,30] Moreover, the effectiveness with which the costly precious metal component is used (i.e., fraction exposed at the surface) is generally low. Some progress has been made towards making nanosized intermetallic catalysts to overcome this limitation. [31] A more effective use of Pd has been demonstrated in single atom alloys (SAA's) where a high proportion of Pd atoms are actually surface atoms. In some cases the Pd atoms in SAA's are assigned as the active site,[32,33] whereas in others they act as a site for hydrogen dissociation with

spillover onto the alloy component where a selective reaction can take place. [34,35,36] There are also a growing number of reports which indicate that surface modifiers can influence selectivity in alkyne hydrogenation. In this regard, both sulphur [37,38,39] and phosphorous [40,41,42] containing compounds have been shown to be effective. Interestingly, with diphenyl sulfide as modifier, it was possible to decompose the organic component of the modifier, retain the sulfur atoms and still supress ethylene hydrogenation activity. [37]

Despite the surge in the number of approaches to enhance performance in alkyne hydrogenation, a number of challenges still remain, perhaps the most pertinent of which is enhanced resistance to deactivation. Therefore the search for improved catalyst formulations now extends beyond metal based catalysts with metal oxides such as CeO_2 [43,44] and In_2O_3 [45] showing promise, albeit at elevated temperature unless doped with other components. [46] Recently, metal sulfides, or more specifically, supported palladium sulfide nanoparticles have been shown to be an excellent hydrogenation catalyst [47,48] with performance attributed to the formation of the Pd_4S phase and isolation of the active Pd sites. [49,50] Whilst these reports focused on a supported Pd_4S phase, it was hinted that similar results could be obtained with a bulk phase palladium sulfide powder. [49] Reports of sulfur being beneficial in heterogeneous catalysis are still somewhat limited [51] Herein, results are presented which demonstrate how a PdS powder evolves and changes with thermal pre-treatment to yield a highly selective alkyne hydrogenation catalyst. Detailed characterisation by XRD, TPR, TEM, EDX, XPS and XAS create an understanding of how the phase composition and crystal structure impacts upon catalytic performance. The deposition of carbon over Pd_4S sample after 50 h reaction were investigated by TPO-MS. Whilst a bulk phase PdS powder does not represent an efficient use of the expensive Pd component, it does serve as an excellent material for creating links which reinforce our understanding of how and why supported sulfide phases are selective in alkyne hydrogenation.

Experimental

Samples

Palladium sulfide powder was purchased from Alfa-Aesar (12674, 99% purity on a metal basis). Sample which was used as received is referred to as 'fresh palladium sulfide'. Portions of the as received sample were subjected to a reduction treatment in a 20% H_2/N_2 mixture (200 ml min^{-1}) for 1 h at 50, 150, 250 or 350°C in the reactor. Samples are denoted as R50, R150, R250 or R350 to reflect the reduction temperature.

Catalyst testing

Gas phase hydrogenation reactions were performed in a continuous flow, fixed-bed microreactor (9 mm diameter, Microactivity Reference, supplied by Micromeritics) using catalyst (20 mg) diluted with

silicon carbide (Aldrich, 200-450 mesh). Single reagent tests were conducted with a mixture of 1.2% acetylene/balance N_2 with 2 equivalents of H_2 co-fed relative to acetylene. Multi reagent tests were conducted in a mixture of 0.6% acetylene/5.4% ethylene/balance N_2 flow with 2 equivalents of H_2 co-fed relative to acetylene and a space velocity of 800,000 h^{-1} based on mass of catalyst. In a typical experiment, a catalyst was tested in the temperature range 50-250°C with 25°C increments with 5 h time on stream (TOS) at each temperature to ensure quantitative measurement of raw conversion/selectivity data reproducibility.

The gas composition at the reactor outlet was determined by GC-FID (PE Clarus 580) using an elite alumina capillary column. Conversion was calculated as the amount of acetylene reacted divided by the amount introduced. Selectivity to ethylene and ethane were calculated as the amount formed (i.e., ethylene $_{out}$ – ethylene $_{in}$) divided by the amount of acetylene reacted. For multi reagent tests a negative ethylene selectivity implies that a fraction of the ethylene co-fed to the reactor also undergoes hydrogenation to ethane. Acetylene is known to form oligomers under reaction conditions. Whilst analysis permitted detection of C4 and C6 products, it was deemed more appropriate to evaluate oligomer selectivity based on a carbon balance [6], since higher molecular weight oligomers may remain adsorbed on the surface, as measured by TPO-MS.

Characterisation

Surface area of samples was measured using a Micromertics Tristar 3000 instrument using N_2 as adsorbate. Samples were first pre-treated by heating to 200°C for 2 h in a flow of N_2. X-Ray Diffraction (XRD) patterns of samples were measured in the range of 2θ=20-85° using an X' Pert powder diffractometer (PANalytical) fitted with a PIXcel1D detector, using Cu Kα radiation and a step size of 0.013° (≈ 15 min acquisition time). The phase compositions were determined by Rietveld refinement using the software HighScore Plus. [52]

Temperature programmed experiments were conducted using a TPDRO 1100 instrument with a TCD detector. The effluent gas stream was then passed into an Eco-Sys portable mass spectrometer (European Spectrometry Services) to determine the gas composition. Temperature programmed reduction (TPR) was conducted by heating a fresh palladium sulfide sample in the temperature range 40-350°C using a heating rate of 5°C min^{-1} in a mixture of 5% H_2/N_2. Temperature programmed desorption (TPD) was conducted by first performing a TPR to 150°C, followed by cooling to 40°C in the same 5% H_2/N_2 mixture. The gas was then switched to N_2 and sample heated from 40 to 350°C using a heating rate of 5 °C min^{-1}. TPR and TPD results are presented per gram of sample and hydrogen consumption quantified based on a response factor determined using a CuO standard. Temperature

programmed oxidation (TPO) in 5% O_2/He at the temperature range 40-500°C using a ramping rate of 5 °C min^{-1} was performed over used samples.

High Resolution Transmission Electron Microscopy (HR-TEM) images were collected using a JEOL JEM-2100 instrument. The particle size and lattice fringes were characterised by analysis of the collected images. The morphology, structure and elemental composition of the samples were examined in several zones using a Zeiss Supra 55 Scanning Electron Microscope (SEM) equipped with an energy dispersive X-ray (EDX) analyser.

X-Ray Photoelectron Spectroscopy (XPS) of samples was performed using a Thermo Fisher Scientific K-alpha$^+$ spectrometer. Samples were analysed using a micro-focused monochromatic Al X-ray source (72 W) over an area of approximately 400 microns. Data were recorded at pass energies of 150 eV for survey scans and 40 eV for high resolution scan with 1 eV and 0.1 eV step sizes respectively. Charge neutralisation was achieved using a combination of low energy electrons and argon ions. The resulting spectra were analysed using CasaXPS peak fitting software and sample charging corrected using the C 1s signal at 284.8 eV as reference.

The Pd and S edge X-ray adsorption spectra (XAS) were collected on the B18 beamline at the Diamond Light Source (Harwell, UK). Measurements of Pd edge XAS were performed using a QEXAFS set-up with a fast scanning Si (311) double crystal monochromator (0.35 eV step size). Samples were diluted with cellulose to optimise the effective edge step for X-ray absorption fine structure (XAFS), pressed into pellets and measured in transmission mode using ion chamber detectors. For fresh palladium sulfide, an average of ten scans were obtained to provide a suitable signal to noise ratio. For the R350 sample, an average of five scans produced suitable signal to noise. All Pd edge XAS spectra were collected concurrently with the appropriate foil placed between ion detectors I_t and I_{ref}. S K-edge XAFS measurements were tested in fluorescence mode using a QEXAFS setup with fast scanning Si (111) double crystal monochromator. Data were collected using a 4-element Vortex Silicon Drift fluorescence detector in the soft X-ray experimental chamber at room temperature. 5 scans per sample were measured with $k_{max}= 9$, and sulfur fluoride was used as the standard for S edge EXAFS analysis. XAS data processing was performed using IFEFFIT 19 with the Horae package (i.e., Athena and Artemis). A fixed input value for the amplitude reduction factor (S02) of 0.85 was chosen based on a known reference material.

Results

Selective hydrogenation of acetylene under competitive and non-competitive conditions

The catalytic behaviour of palladium sulfide reduced at four different temperatures was first evaluated using a simple acetylene/hydrogen mixture with results displayed in Figure 1. Note that for each sample, the reaction began with a period at 50°C, prior to increasing the reaction temperature sequentially in 25°C increments up to 250°C (5h TOS permitted at each temperature). Several observations can be made by first focusing on the data collected at reaction temperature of 50°C. Performance changes markedly with TOS for R50, R150 and R250 samples, whereas R350 sample appears far more stable. This may be because samples reduced at lower temperature undergo physical change during time on stream (see later). With regards to the initial activity, there is a clear trend between reduction temperature and acetylene conversion with activity increasing in the following order: R350 > R250 > R150 > R50, suggesting differences in structure for PdS samples reduced at these four different temperatures. In terms of selectivity, all samples produce ethylene as the major product with higher selectivity observed for samples which showed lower activity. As temperature was increased in the range 75-175°C, the samples showed marked differences. R50 exhibits low selectivity to ethane and higher selectivity to oligomers, whereas R150, R250 and R350 tend to produce more ethane than oligomers. Once the reaction temperature reached 200°C, all samples produce similar product distributions, which suggests that samples are structurally and physically similar. Interestingly, ethylene selectivity appears to reach a plateau for all samples with only lesser amounts of ethane and oligomers formed beyond 200°C. For example, at 250°C, R350 displays a maximum selectivity of 82.8% with little ethane (9.5%) and oligomers (7.7%). These findings would suggest that treatment at higher temperature, either in reaction or by pre-reduction, is conducive to producing a more selective alkyne hydrogenation catalyst.
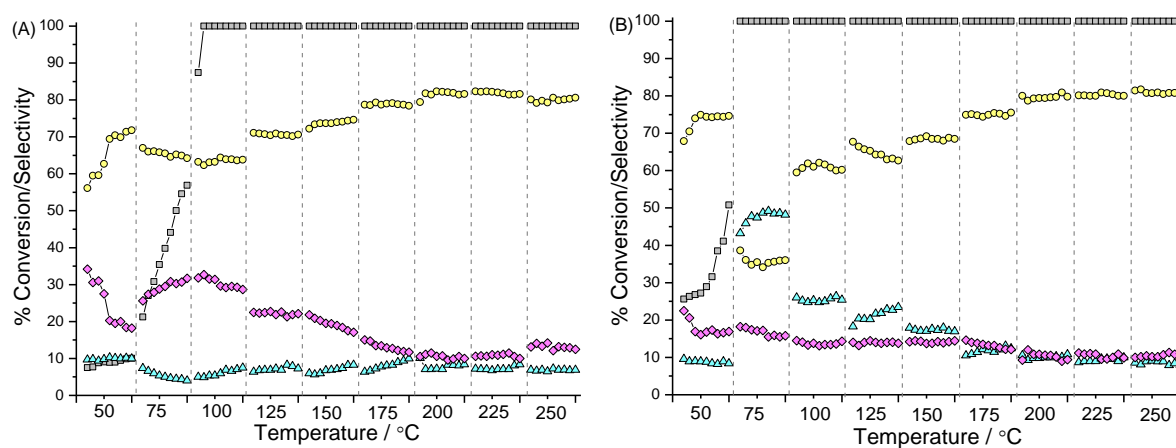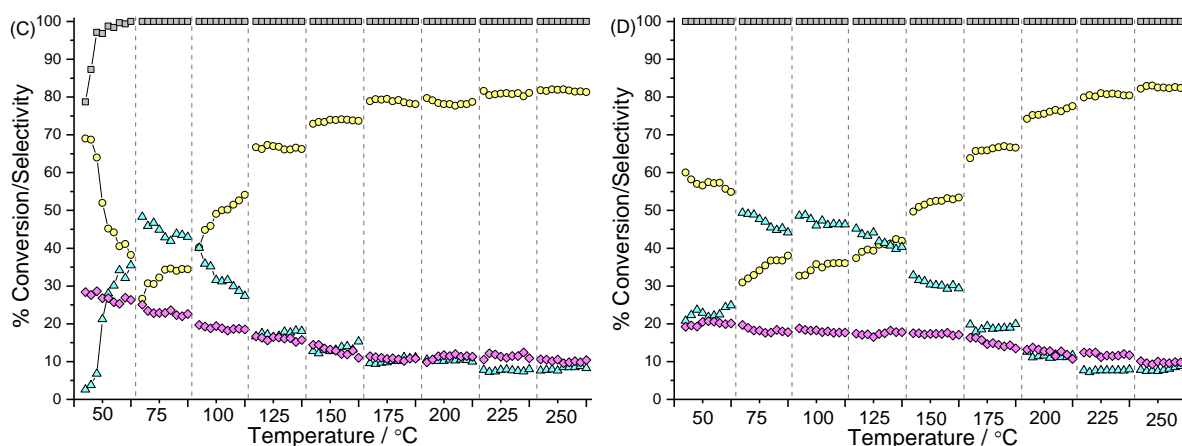
Figure 1. Acetylene conversion (grey squares) and product selectivity to ethylene (yellow circles), ethane (cyan triangles) and oligomers (pink diamonds) as a function of temperature. Data points at each temperature correspond to 5 h time on stream in order to ensure quantitative measurement of raw conversion/selectivity data reproducibility. (A) R50, (B) R150, (C) R250 and (D) R350 (1 bar, 2-fold excess of H, SV=800,000 h^{-1}, in the acetylene/hydrogen feed).

R350 sample was selected for further testing on the basis of characterisation results (see later), since links between structural properties and catalytic performance could be readily determined. Catalytic results obtained under competitive conditions (i.e., both acetylene and ethylene present in the feed gas), more akin to those encountered in industry [6] are summarised in Table 1. It is important to highlight a few points. Firstly, a negative ethylene selectivity implies that a fraction of the ethylene present in the feed gas has undergone hydrogenation. Secondly, at all temperatures, 100% conversion of acetylene was observed, despite the use of a space velocity 2 orders of magnitude higher than that typically used in industry. [6] This does, in a qualitative sense, suggest that R350 is highly active. Quoting performance at complete conversion is important because industrially, approximately 99.95% acetylene conversion is necessary to reach the requisite ethylene purity. In addition, selectivity at lower conversion may reflect thermodynamic selectivity (i.e., acetylene adsorbs more strongly than ethylene) as opposed to whether or not a catalyst is truly selective. In agreement with simple acetylene/hydrogen tests, R350 sample produces significant amounts of ethane at low reaction temperatures (Table 1). However, over-hydrogenation decreases significantly at 200°C with ethylene becoming the major product. At 250°C, ethylene selectivity of 90% was obtained, which compares well with state of the art materials such as ceria (81% ethylene selectivity at 86% acetylene conversion - 250°C, 30 fold excess of H$_2$), indium oxide (≈90% ethylene selectivity @ 30% conversion - 350°C, 30 fold excess of H$_2$) and monometallic Pd catalysts (Table S1).[43, 46,53, 54,55]

Table 1. Acetylene conversion and product selectivity to ethylene and ethane at different reaction temperatures over R350 sample [a]

Performances	100°C	150°C	200°C	250°C
Conversion of acetylene (%)	100	100	100	100
Selectivity to ethylene (%)	-17.2[b]	-1.1[a]	54.4	90.9
Selectivity to ethane (%)	96.7	98.1	45.6	9.1
Selectivity to oligomer (%)[c]	20.5	3.0	0	0

[a] Reaction conditions: 1 bar, 2-fold excess of H_2, SV = 800,000 h^{-1}, 0.6% acetylene and 5.4% ethylene in feed gas.

[b] Note that a negative selectivity to ethylene implies that a fraction of ethylene present in the feed gas was hydrogenated.

[c] Oligomer selectivity including C4 and C6 products was evaluated based on a carbon balance (100 $\pm$2%). Carbon contents of higher molecular weight oligomers which may remain adsorbed on the catalysts were 1.7 wt. %, measured by TPO-MS.

Hydrogen consumption during reduction.

Figure 2A shows the H_2-TPR profile (top) of fresh palladium sulfide sample along with the corresponding MS profile of gas phase species (bottom). A strong peak in the temperature range 30-150 °C was observed due to hydrogen consumption. This is consistent with the MS profile which shows a decrease in ion intensity associated with H_2 (m/z = 2). Quantification of this peak suggests that 1.04 mmol of H_2 is consumed per gram of sample which equates to a H_2: PdS ratio of 0.15. At *ca.* 175°C, a negative peak was observed. Based on relative thermal conductivities, a negative peak would normally be associated with release of H_2 from a sample during a TPR. However, the corresponding MS profile suggests that small amounts of H_2S (m/z = 34), SO_2 (m/z = 64) and H_2O (m/z = 18) are also released. With all three of these gases, a positive peak would be expected from the TCD detector using N_2 as carrier gas. The net effect would be that the magnitude of the signal associated with H_2 release at *ca.* 175°C is hidden. To separate out these effects, a sample was exposed to H_2 up to 150°C before being cooled down to 40°C and a N_2-TPD performed. In this case, a much larger negative peak was observed (Figure 2B–top) along with a sharp MS signal associated with H_2 and small amounts of SO_2 and H_2O (Figure 2B–bottom). Comparison of the peak area of the negative peak in Figures 2A and 2B show that in the latter case, the peak was almost 5 times larger. This would appear to be consistent with the interpretation that in Figure 2A, the peak is a composite of all the gases being released. Returning to the H_2-TPR (Figure 2A), as temperature was increased beyond 225°C, a sharp increase in the MS signal

associated with H_2S was observed. There was no hydrogen consumption at this point, suggesting that H_2S was formed from hydrogen consumed at lower temperature and stored in the material until a critical temperature for desorption had been reached. However, were that the case, H_2S should be observed at higher temperature in Figure 2B. Since no H_2S was detectable at any point during N_2-TPD it is likely that H_2S is predominantly formed at temperatures above 225°C.
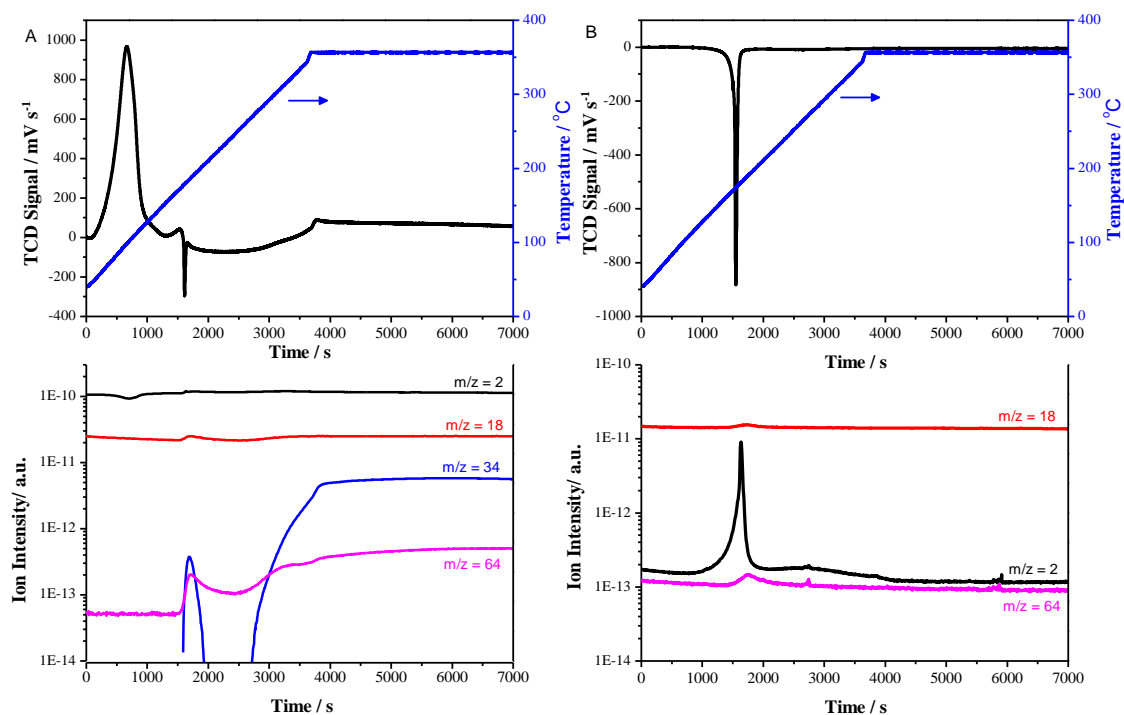
Figure 2. (A) TPR profile (top) and corresponding MS profile (bottom) for fresh palladium sulphide sample. (B) TPD profile (top) and corresponding MS profile (bottom) for sample heated to 150°C in 5% H_2/N_2 and cooled before N_2 TPD. m/z ratios of 2, 18, 34 and 64 are attributed to H_2, H_2O, H_2S and SO_2, respectively.

**Phase composition following reduction**

Based on TPR experiments, it is expected that the composition of samples will change depending on pre-reduction temperature. As well as this, it is known that palladium sulfide can exist [56] in a number of different phases including PdS, $Pd_{16}S_7$ and Pd_4S (note that transformation from PdS → $Pd_{16}S_7$ → Pd_4S, samples gradually become increasingly palladium rich). In order to investigate if and how phase composition changed with reduction temperature, a detailed XRD study was performed. Diffraction patterns for sample reduced at different temperatures are presented in Figure 3 along with reference patterns for the most common palladium sulfide phases. No discernible features were observed in the pattern of R50, or that of fresh palladium sulfide (not shown), suggesting that both materials are amorphous. In general, increasing the pre-reduction temperature resulted in materials which were

more crystalline and this was accompanied by particle growth (TEM data discussed later). Reduction at 150°C results in the emergence of peaks at 2θ = 30.3°, 31.07°, 33.95°, which were roughly in agreement with the standard PdS (PDF 25-1234). In order to further quantitatively analyse the phase compositions of four reduced materials, Rietveld refinements were carried out based on the structural models ($P4_2/m$, $P\overline{4}2_1c$ and $I\overline{4}3m$), [52] and the results are listed in Table 2. Generally, small reliability factors (R < 2%) were determined, which indicates that these refinements were satisfactory. For R150 sample, the refinement fit was poorer but suggested that the refined weight percent of PdS phase was 48.6 wt. %, along with the presence of a larger amount of $Pd_{16}S_7$ (51.4 wt. %). A far more defined pattern was observed for R250 sample (Figure 3) and refinement suggested a shift towards palladium rich phases (Table 2) consistent with loss of sulfur observed at higher temperature during H_2-TPR (Figure 2). Perhaps unsurprisingly, this trend continued for R350 sample which can be considered as a largely pure phase Pd_4S (94.6% refined weight percent). Based on XRD, the following phase transformation with increasing reduction temperature can be expected:

$$\text{Amorphous palladium sulfide} \rightarrow PdS \rightarrow Pd_{16}S_7 \rightarrow Pd_4S$$

As the change in phase composition appears to be largely controlled by temperature in the presence of H_2, it is expected that both R50 and R150 samples would be liable to undergo phase changes during catalytic reaction (i.e., as the temperature is increased beyond the pre-reduction temperature). In contrast, R250 and in particular R350 should be far more stable, which explains why their reactivity trends appear similar (Figure 1). In order to validate this hypothesis, the XRD pattern of used R250 and R350 samples were further collected. After subtraction of the SiC diluent contribution, the XRD pattern looked identical to the fresh samples, confirming no further phase change occurred (Figure S1).
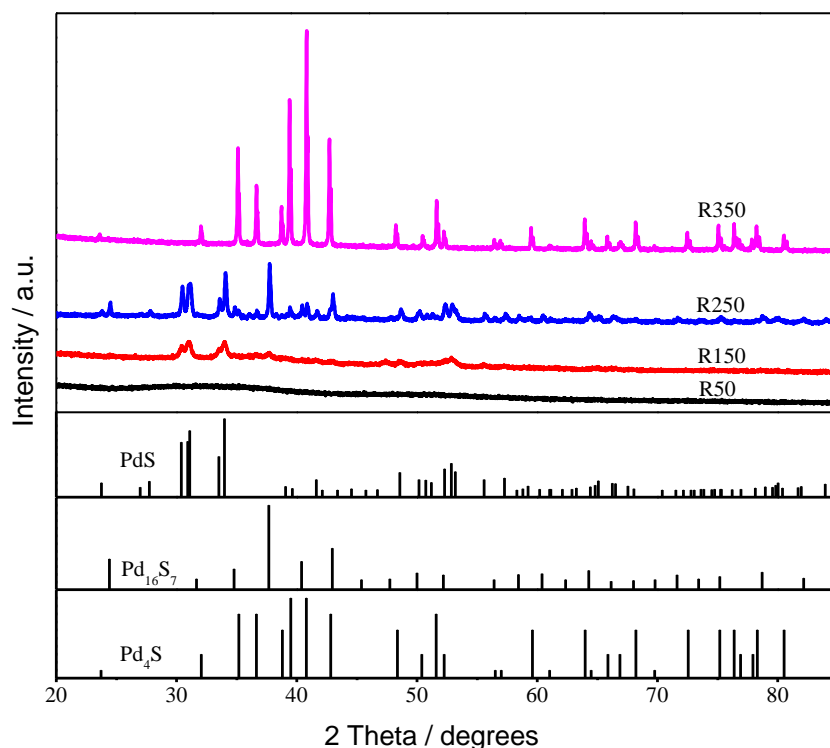
Figure 3. XRD patterns of R50, R150, R250 and R350 samples. Reference patterns for XRD patterns for PdS, $Pd_{16}S_7$ and Pd_4S are included.

Table 2. Composition of palladium sulfide samples determined by XRD, EDX and XPS.

| Sample	BET surface area $(m^2 \, g^{-1})$	XRD phase composition[a]			XRD composition		EDX composition		Bulk phase Pd:S ratio[b]	Bulk phase Pd loading (wt. %)[c]	Surface Pd:S ratio[d]
		PdS	$Pd_{16}S_7$	Pd_4S	Pd (wt. %)	S (wt. %)	Pd (wt. %)	S (wt. %)			
R50	20.7	-	-	-	-	-	79.9	20.1	1.2	75.9	1.0
R150	19.7	48.6	51.4	0.0	82.7	17.3	83.1	16.9	1.5	81.3	1.0
R250	3.6	27.4	58.2	14.4	85.7	14.3	85.3	14.7	1.8	83.6	1.6
R350	1.5	5.4	0.0	94.6	92.1	7.9	92.5	7.5	3.1	90.2	3.0

[a] Determined by XRD
[b] Determined by EDX
[c] Determined by ICP
[d] Determined by XPS

Microscopy study following reduction

The micro-structure of PdS nanoparticles reduced at 50, 150, 250 and 350°C, were evaluated by HRTEM (Figure 4). Sample subjected to reduction at 50°C shows a very small particle size (Figure 4–A₁

and A_2) and appears largely amorphous at high magnification (Figure 4–A_3 and A_4), consistent with XRD measurements (Figure 3). In comparison, R150 sample appears to have undergone agglomeration resulting in increased particle sizes (Figure 4–B_1). In agreement with expectations based on XRD measurements, R150 sample exhibits lattice fringes which may be attributed to both PdS (Figure 4–B_4) and $Pd_{16}S_7$ (Figure 4–B_3) phases. Increasing the reduction temperature to 250 or 350°C further increased the crystallinity and particle size (Figure 4–C and D), and this latter aspect can be clearly seen in the diminished BET surface areas (Table 2). With the R250 sample, lattice fringes were observed which can be attributed to multiple palladium sulfide phases (Figure 4–C_3 and C_4). Consistent with XRD measurements, the predominant lattice fringes for R350 sample are associated with the Pd_4S phase (i.e., d = 0.228 nm, (210)–Figure 4–D_4).
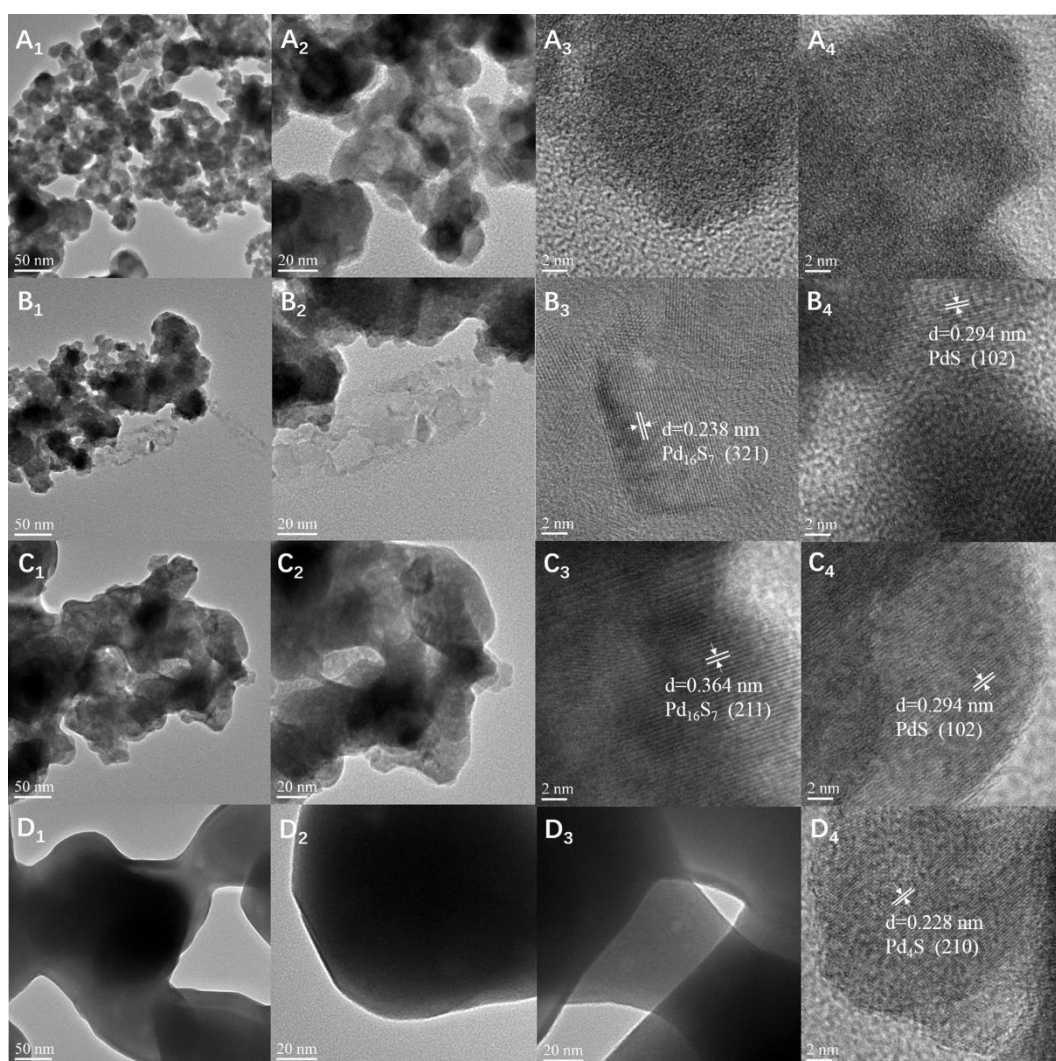
Figure 4. HRTEM images of (A) R50, (B) R150, (C) R250 and (D) R350.

In order to assess sample uniformity, EDX mapping was performed in several zones to ensure analyses were representative of the whole sample (Figure 5 and Figure S2). As observed with TEM, increasing pre-reduction temperature tends to result in agglomeration of the palladium sulfide. The insets of Figure 5 illustrate the elemental mapping scan of all four samples and the images demonstrate a homogeneous distribution of Pd and S elements across the particles. Therefore, whilst there is evidence from XRD and TEM that the phase of each individual particle may be different, it would appear unlikely that there are particles which are exclusively composed of either palladium or sulfur. The weight percent of palladium and sulfur was measured from EDX and is presented in Table 2 and S2. As expected, as reduction temperature is increased, the samples become richer in palladium as a result of the loss of sulfur (Figure 2). For example, R50 sample is composed of 20.1 wt. % sulfur which decreases to 16.9 and 14.7 wt. % for R150 and R250 samples, respectively. Interestingly, there is a noticeable decrease in the amount of sulfur upon going from R250 to R350, in-spite of relatively little change to catalytic performance (compare Figure 1c and d). Similar catalytic performance would indicate that the surface structure/composition is likely to be similar. As a result, it is thought the additional loss of sulfur with heating to 350°C is associated with loss from the bulk of particles as opposed to the surface. Based on the phase composition determined from XRD, the corresponding Pd and S weight percent was calculated for R150, R250 and R350 samples (it was not possible to calculate for the amorphous R50). Excellent agreement was obtained between the composition determined by XRD, EDX and ICP (Table 2), confirming both techniques give complimentary information for these samples.
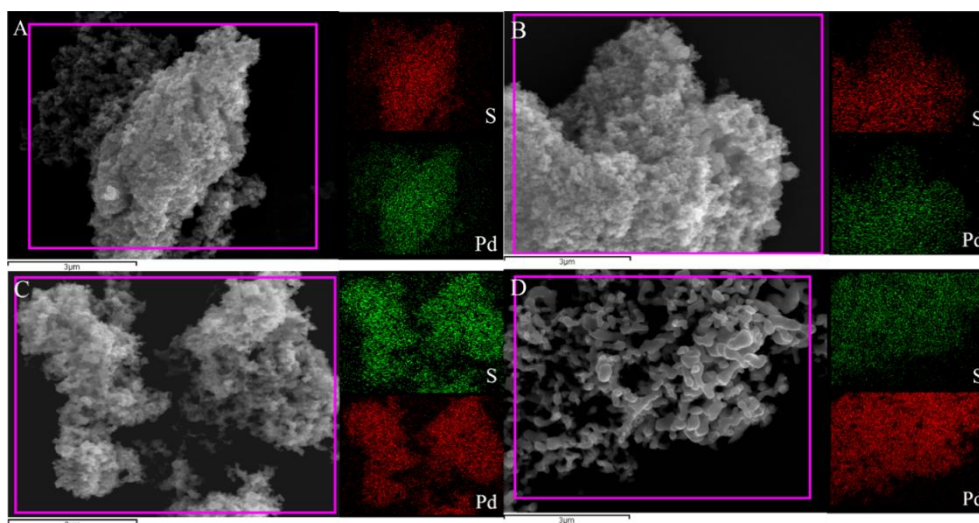

Figure 5. SEM-EDX images of (A) R50, (B) R150, (C) R250 and (D) R350. The insets show the S (green) and Pd (red) elemental mapping of the area within the pink square.

Surface composition following reduction

Whilst XRD, TEM and EDX measurements were all in agreement, they largely provide insight into the bulk structure which may or may not be the same as the surface. Therefore, in order to obtain information specific to the surface and near surface region, XPS measurements were collected (Figure 6). The doublet Pd $3d_{5/2}$ and $3d_{3/2}$ of fresh PdS appear at~336.8 and 342.0 eV, respectively, suggesting that only Pd^{2+} exists. With the reduction temperature increasing, it is noticed that the Pd $3d_{5/2}$ peak shifts from 336.8 eV (in R50) to 335.5 eV for the reduced catalyst at 350 °C. Given that reduced palladium shows a $3d_{5/2}$ peak near 335.2 eV and the equivalent peak in palladium oxide occurs at *ca* 336.7 eV, it is possible to make comment regarding the oxidation state of Pd in palladium sulfide. For example, reduction at low temperature results in Pd atoms retaining a more positive formal charge, whereas reduction at 350°C sees Pd atoms with a near neutral charge. This observation is logical since in 'PdS' the formal charge of Pd would be +2, whereas in 'Pd_4S' the formal charge would be +0.5 (assuming S^{2-} in both cases). The shift is also in agreement with literature. Bachiller-Baeza *et al*. [47] reported that $PdSO_4$ impregnated on a carbon support produced a shift in the Pd $3d_{5/2}$ peak from 337.3 to 335.5 eV during a reduction treatment, which formed Pd_4S.

The S $2p_{3/2}$ region (Figure 6B) of fresh PdS, R50, R150 and R250 shows a clear signal, while the peaks in R350 sample exhibit lower intensity since this contains the smallest amount of sulfur after thermal treatment (see Table 2). The sulfur peak for fresh PdS and samples reduced at 50, 150 and 250 °C is very broad (160-164 eV), implying it may be composed of more than one component. Typically, the $2p_{3/2}$ peak for a sulfide like species is observed at 161.5 eV [57] and overlap between the $2p_{3/2}$ and $2p_{1/2}$ can result in a broad, unresolved doublet. In contrast, an analogous metal sulfate would exhibit a peak at 169 eV. [47] It is therefore likely that the broad peak observed in the XP spectrum of fresh PdS, R50, R150 and R250 is an unresolved doublet associated with a sulfide peak. However interestingly, the binding energy of broad peak observed in R350 is between 162-166 eV, which was also similar with that reported by Singh *et al*. [58]. In that case, the authors did not attribute the signal to a sulfide species as such, but opted to describe the Pd_4S structure as an 'alloy type compound'. Based on the spectra presented in this work, it appears reasonable to assume that some formal charge exists on the Pd and S atoms (i.e., the binding energy of Pd is similar with the expected for Pd^0 and the binding energy for S is higher than S^{2-}). Table 2 also shows the surface Pd:S ratio as determined by XPS along with the bulk phase ratio determined from EDX. There is a rough agreement between the two methods suggesting that the bulk phase and surface are closely related.
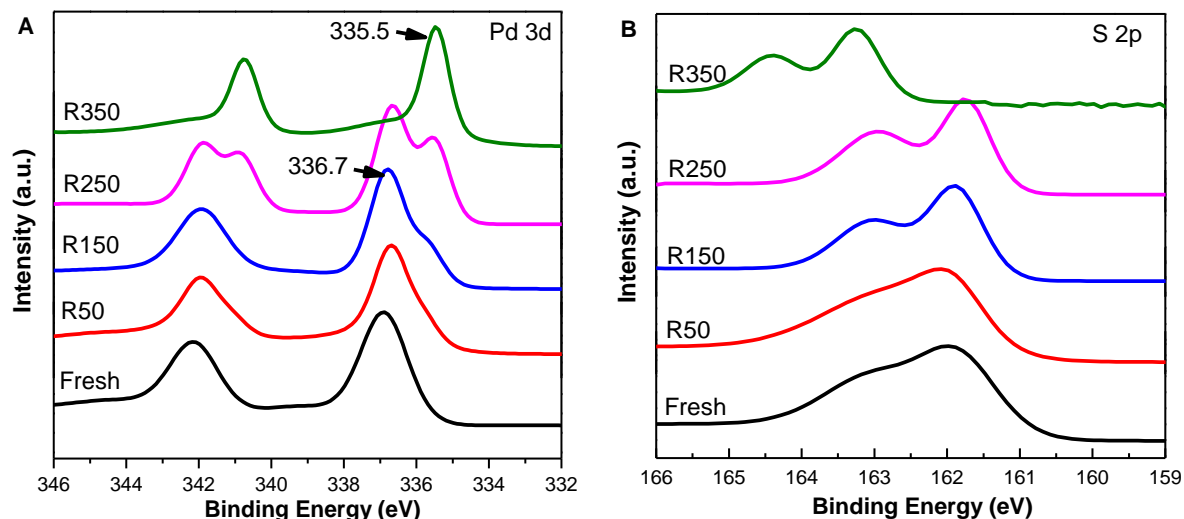
Figure 6. XP spectra of Pd 3d (A) and S 2p (B) regions.

Insights from X-ray absorption spectroscopy

To better understand the structure-performance relationship for palladium sulfide, X-ray absorption spectroscopy measurements were conducted. The Pd K edge X-ray Absorption Near-Edge Structure (XANES) of fresh palladium sulfide (i.e., unreduced), R350 and a Pd reference foil is presented in Figure 7. There is a difference between the absorption edges of fresh sample and R350, and the later appears more similar to that of Pd foil, which would imply that the oxidation state in both cases is similar. This would appear to be consistent with XPS measurements, suggesting the Pd oxidation state was close to Pd^0. Moreover, it is worth noting that there is a clear change of white line owing to s-p-d hybridization.[59] Based on the reported, a less intense white line for palladium sulfides corresponds to more d-electrons with respect to the Pd foil, [60] which is in accordance with XPS analysis. Additionally, the presence of continuum resonance (CR) in the range of 24385-24390 eV, associated with 4f Pd-like states [61,62] contributes to the differences between the spectrum of palladium sulfides and Pd foil. With respect to the reference sample, a small shift of CR toward low energy is visible in the palladium sulfides, indicating the increase of the Pd–Pd distance. [63] This is most likely ascribed to the introduction of S atoms.
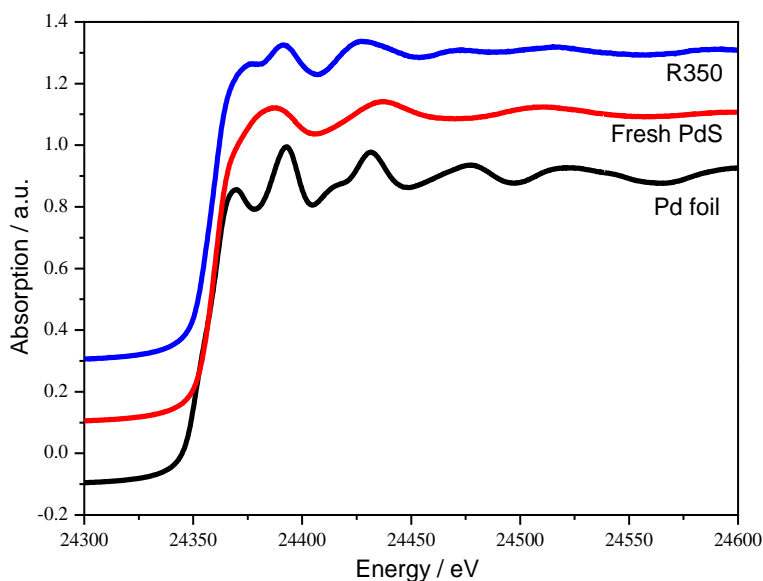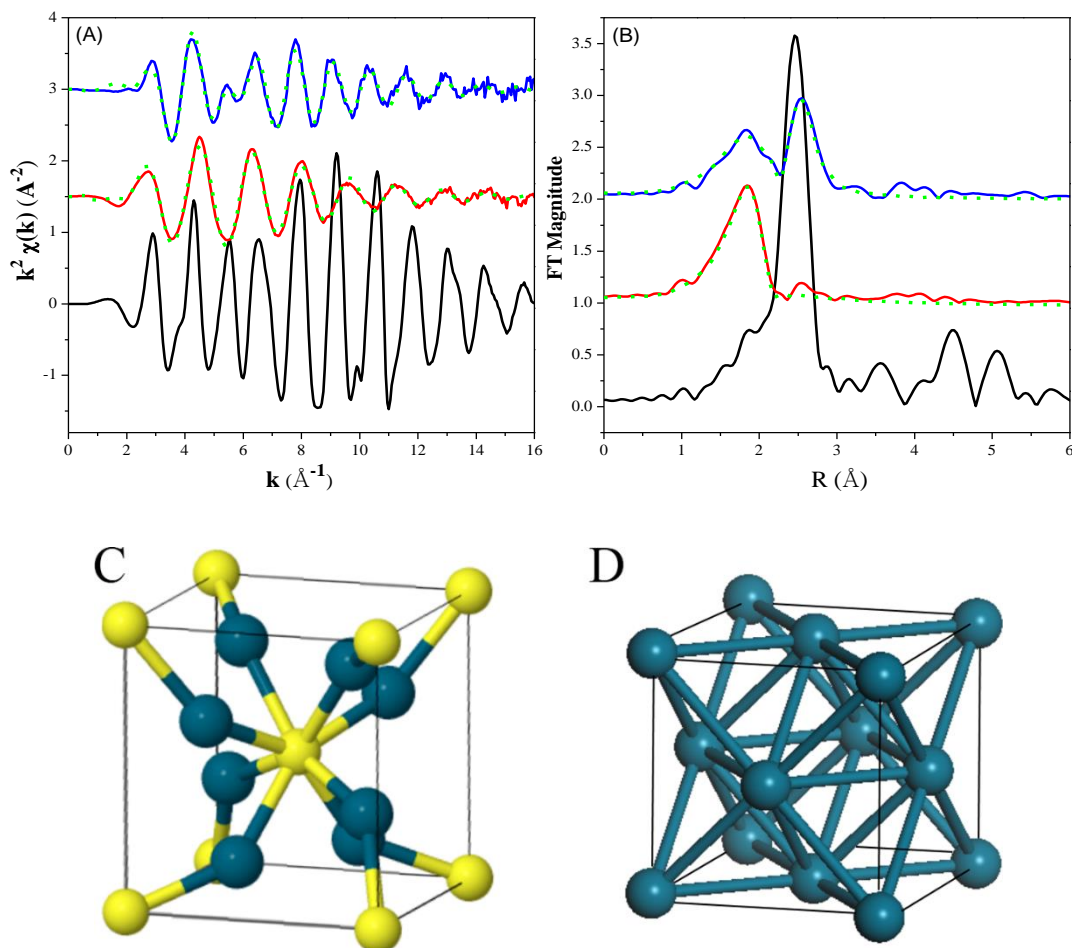
Figure 7. Normalized Pd K edge XANES spectra for fresh palladium sulfide (red), R350 sample (blue) and reference Pd foil (black).

Figure 8 illustrates the k^2-Weighted Pd K-edge EXAFS oscillations (A) and the corresponding Fourier transforms (B) to give detailed insight into the atomic arrangement of Pd atoms for both samples. The fitting curves for χ^2 (k) data (dashed line in Figure 8A) fit the experimental data for both fresh and R350 samples well up to *ca*. 15 Å^{-1}. As presented in R space (Figure 8B), two characteristic peaks were observed in the range of 0.12-0.30 nm ascribed to the scattering of Pd-S and Pd-Pd atomic pairs. Furthermore, the fitting for the Fourier-filtered spectrum were performed by considering the contributions of Pd–S and Pd–Pd shells. The quantitative parameters of the nearest coordination number (N), atomic distance (r), the difference in the threshold energy (ΔE) and Debye-Waller factor (σ) are summarized in Table 3. For the fresh sample, only Pd-S scattering contributions were found with an atomic distance of 0.232 nm and a coordination number of *ca*. 3.5. Any attempt to include Pd-Pd scattering contributions at longer atomic distance decreased the quality of the fit. For R350 sample, contributions from both Pd-Pd and Pd-S scatterings were present. The shortest atomic distance was associated with a Pd-S interaction (0.230 nm, coordination number *ca*. 1), consistent with the results of the k^2-Weighted S K-edge EXAFS (Figure S5). There were, however, more Pd-Pd interactions (coordination number *ca*. 3) but with at a larger atomic distance of 0.279 nm. The atomic distance for the Pd-Pd interaction in the reference foil was found to be shorter at only 0.275 nm. The Pd-S and Pd-Pd interatomic distances measured in this work are comparable to those determined previously by Murayama *et al*. [64] by EXAFS. In that work, Pd-S and Pd-Pd distances of 0.233 and 0.279 nm, respectively, were reported for Pd clusters containing thiolate ligands. Similarly, the interatomic distances found here fit within the range determined experimentally by crystallography [65] and by DFT

calculations [66] for the Pd_4S structure, suggesting that Pd atoms in Pd_4S are subjected to geometric effects/site isolation, relative to Pd atoms within nanoparticles. The 3D models (Figure 8C and D) confirm this conclusion that Pd atoms within Pd_4S possess exclusively S atoms as surface neighbours.

Figure 8. (A) k^2-Weighted Pd K-edge EXAFS oscillations and (B) Fourier transforms spectra of fresh palladium sulfide (red), R350 sample (blue) and reference Pd foil (black). Dotted lines represent the best fitting curves in the EXAFS analysis. 3D structure of (C) Pd_4S and (D) Pd metal.

Table 3. EXAFS parameters fitted for fresh PdS and R350 samples

Sample	Shell	N^a	r^b (nm)	ΔE^c (eV)	σ^d
PdS	Pd-S	3.47±0.06	0.232±0.003	1.35±0.40	0.0057±0.0004
R350	Pd-S	0.978±0.17	0.230±0.001	-1.46±0.40	0.0054±0.0016
	Pd-Pd	2.978±0.37	0.279±0.005	-1.46±0.40	0.0081±0.0008

[a] Coordination number (N)   [b] Atomic distance (r)

Stability testing

To demonstrate the exceptional stability of catalysts while operating at high conversion, time-on-stream analysis for the four PdS catalysts was conducted under non-competitive conditions (Figure 9). 83% selectivity to ethene was observed for R350 at 100% acetylene conversion without significant shift in activity or product selectivity during the 50 h reaction. A slight decrease of selectivity from 81 to 77% was found in R250, and a more significant loss for R150 (from 79 to 65%) and R50 (from 79 to 54%) was observed. Furthermore, in order to extend these tests to more industrial-like conditions, the stability test over R350 was also performed in mixed alkyne/alkene feeds (Figure S3). During 50 h on stream, the activity and selectivity essentially remained constant (100 and 90%, respectively) thus confirming the stable performance for R350 catalyst.
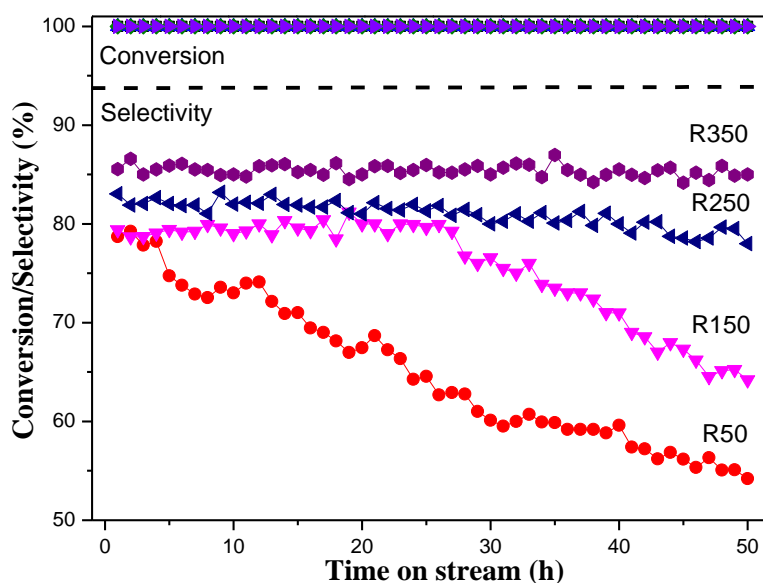
Figure 9. Acetylene conversion and selectivity *versus* time on stream over the PdS catalysts (GHSV: 800,000 h^{-1} at 250 ^{o}C).

It is well known that changes of catalyst structures and deposition of carbon result in deactivation of hydrogenation catalysts. In this work, the structural stability of PdS samples was confirmed by XRD and HRTEM with good agreement between the fresh and used PdS samples (Figure S1, S3 and S4). To compare the extent of accumulation of any carbonaceous residues, carbon contents were quantified after reaction using TPO-MS data and the values for R50, R150, R250 and R350 were 4.7, 2.4, 1.3, and 1.2% of the catalyst weight, respectively. Moreover, as shown in Figure 10, the CO_2 evolution profile for PdS samples occurred at different temperature, corresponding to several types of coke species. The

peak located in the range of 250-300°C is attributed to unstructured carbon, which does not affect the reaction even though they may be in contact with the metal particles since the combustion is most readily affected. [67, 68] The second peak (300-450°C) can be attributed to the combustion of amorphous coke, a precursor of graphitic carbon with a structure of C_xH_y, the accumulation of which provokes considerable steric hindrance, reducing the availability of hydrogen and/or acetylene. [68] Compared with R50 catalyst, the peak area of amorphous coke on R350 is 70% less and the peak is shifted to lower temperature, indicating the preferable resistance against carbonaceous build up over this sample thus explaining its superior stability.
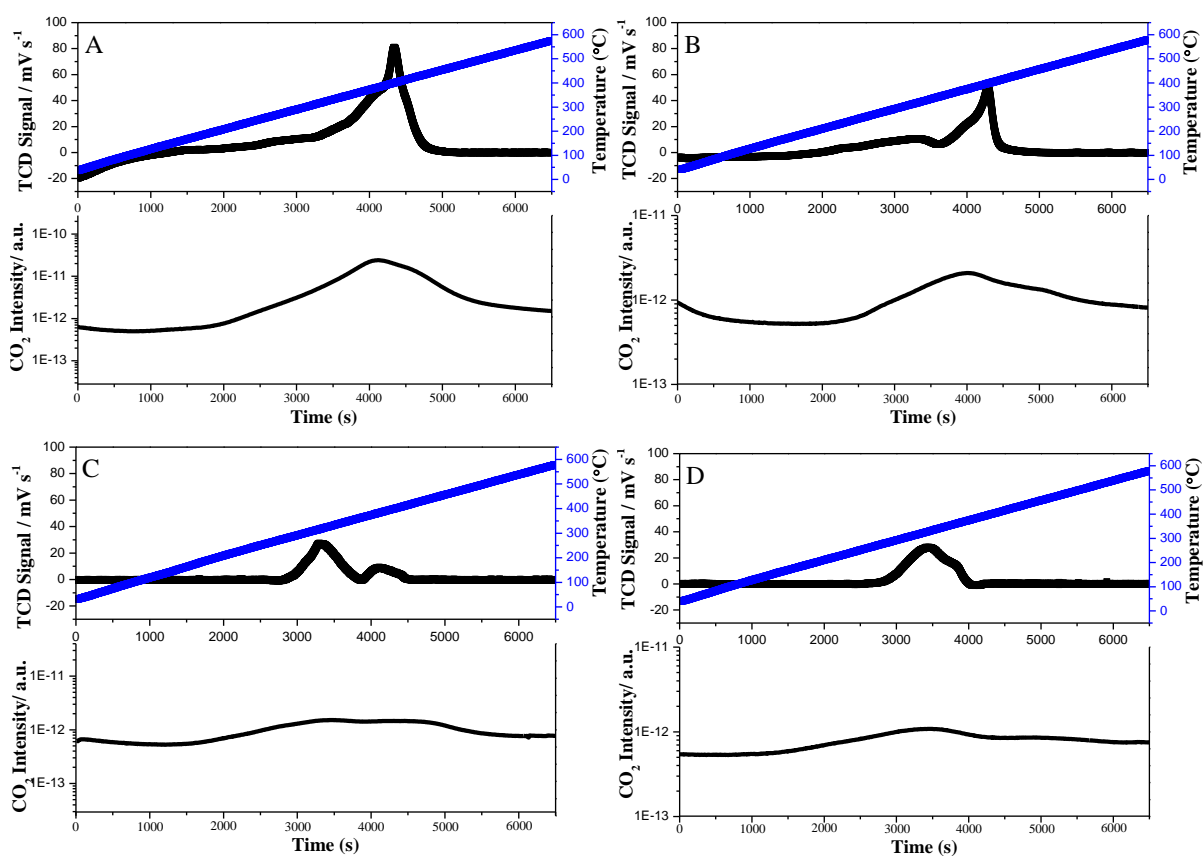
Figure 10. TPO profiles (top) and corresponding MS profiles (bottom) for (A) used R50, (B) used R150, (C) used R250 and (D) used R350 after 50 h test in the acetylene/hydrogen feed.

Discussion

Evolution of the palladium sulfide phase

The fresh palladium sulfide material used in this work is amorphous and has a structure which is largely dominated by Pd-S interactions (Table 3). Upon heating in a hydrogen containing atmosphere, the sample undergoes significant changes in terms of the composition, phase, crystallinity and surface area (Table 2). The extent to which these occur depend greatly on reduction temperature. At low

temperature (≈ 50°C), it is clear that hydrogen interacts with the palladium sulfide, perhaps by forming a hydride type phase as previously reported. [50] However, this results in only a minor change in crystallinity and composition. Increasing the reduction temperature to 150°C sees the onset of sulfur loss as H_2S or SO_2 (Figure 2A) from the surface, consistent with a shift in the composition measured by EDX (Table 2). At this temperature, the sample becomes less amorphous and XRD/TEM suggest a mixture of phases (PdS and $Pd_{16}S_7$) (Figures 3 and 4). Once the reduction temperature reaches 250°C, sulfur is predominantly lost as H_2S (Figure 2A). XRD suggests a gradual shift in the phase composition from a sulfur rich PdS phase to a sulfur lean Pd_4S phase (*via* $Pd_{16}S_7$ as an intermediate).

Given that by 250°C, considerable particle growth has occurred, it seems relevant to consider the transformation on a macroscopic scale. Hydrogen and sulfur must diffuse through the structure until they meet and react. In principle, this could occur by S atoms migrating from the bulk to the surface. However, given that palladium sulfides are known to be permeable to hydrogen,[69, 70] it seems more likely that hydrogen diffuses from the surface into the bulk to find a S atom. That being the case, one would expect that sulfur atoms are abstracted from surface and near surface sites first. This would result in the sulfur deficient phase tends to be on the surface and near surface region relative to the bulk of a particle. Reduction at 350°C seems to provide the system with sufficient energy to convert to a largely pure phase (Figure 3). Only a small fraction (5.4%) of the sample remains as PdS according to XRD. This could be because the core of larger particles is still rich in sulfur, however, if that were the case then the intermediate $Pd_{16}S_7$ phase should be observable. It therefore seems more likely that there is a small amount of PdS which is more thermally stable.

Implications of the phase transformation on activity

Pre-reduced samples were used to collect the catalytic data presented in Figure 1. This is significant as reaction data was collected while increasing the temperature from 50 to 250°C. In other words, R50 and R150 samples would be expected to continue to undergo change during reaction as the feed gas contains hydrogen. As a result, the only data points which can be directly correlated with characterisation results would be those collected at a reaction temperature of 50°C, assuming that R50 and R150 samples undergo no further change under reactions conditions. In terms of activity, as the amount of Pd_4S increases, the activity also increases (i.e., R350 is most active at 50°C) despite particle growth and a corresponding decrease in the relative number of surface sites. However, it was worth noting that the phase composition gradually shifted from a palladium-lean PdS phase to a palladium-rich Pd_4S phase (Table 2), and the oxidation state of Pd changed from positive to a near neutral charge (Figure 6 and 7) with an increase in the reduction temperature, which was similar with the properties of Pd metal/alloy. [58] Based on the above results, it is believed that sample reduced at

350°C possesses a greater ability to activate hydrogen than R50, R150 and R250 due to this metallic characteristic [47, 69] and consequently contributed to the enhanced activity.

Implications of the phase transformation on selectivity

From Figure 1 it would be tempting to assume that PdS and $Pd_{16}S_7$ phases are more selective than Pd_4S. However establishing clear links between palladium sulfide phase and selectivity at 50°C is not trivial since ethylene selectivity is strongly influenced by conversion. [6] This is because over-hydrogenation typically occurs more readily at high acetylene conversion/low acetylene coverage. At reaction temperatures above 50°C, the performance of R50, R150, R250 and R350 samples become more equivalent. Indeed, all samples display ethylene selectivity of *ca*. 80% at 100% conversion at 250°C (Figure 1). Given that the selectivity of the R350 sample can be directly related with the presence of the Pd_4S phase, it seems reasonable to assume that the same phase dominates the surface zones of the remaining samples when under reaction at these higher temperatures. In other words, sulfur is initially stripped away from the surface and near-surface layers, during exposure to hydrogen at the elevated temperatures necessary to form Pd_4S.

XAS results provided detailed information about the environment around Pd atoms in R350 sample (Table 3 and Figure 8). The results are largely in agreement with the crystal structure reported for the Pd_4S phase [65] with the nearest neighbour for a Pd atom being a single sulfur atom at 0.230 nm (Table 3). Pd-Pd interactions are more prominent but, importantly, are at an elongated distance (0.279 nm) relative to monometallic Pd (0.275 nm). [70] DFT calculation and experiment results in the literature indicate that the larger Pd-Pd interatomic distance in Pd_4S, relative to Pd nanoparticles acts partly to create site isolation (no larger than Pd3), which is beneficial for improving alkyne hydrogenation performance. [27-30, 71] In this work, a similar effect is thought to be responsible, in part, for the exceptional selectivity of the Pd_4S phase, compared with monometallic Pd catalysts. However, samples with PdS structure (R50, R150 and R250) show lower selectivity of ethylene even though they, in principle, offer better site isolation (Figure 8), indicating that the small ensemble size (geometric effect) cannot be considered as the sole reason for the differences in the catalytic selectivity observed for PdS samples.

TPR-MS results show that thermal treatment in hydrogen strips sulfur from palladium sulfide during the reduction process (Figure 2). The sulphur, as the neighbour on the surface of Pd_4S catalyst, perturbs the electronic structure of Pd, leading to the valence state of Pd changing from a more positive charge to a near neutral charge, consistent with XPS and EXAFS analysis. Therefore, in contrast to R50, R150 and R250 with PdS structure, the surface Pd atoms in the Pd_4S sample (R350) possesses

much higher electron density. Based on reports in literature [72,73], negatively-charged Pd favours the desorption of ethylene, thus improving the selectivity.

In summary, a possible mechanism considering site isolation and the role of lost sulfur over Pd_4S catalysts is proposed. In detail, in the term of the samples with small ensemble size (no larger than Pd3), C_2H_2 prefers to coordinate on two adjacent Pd atoms, facilitating formation of C_2H_4 through an ethylene-like C_2H_3Pd intermediate, whereas ethylene adsorbs on a Pd atom in π configuration with a low adsorption energy. [30] Moreover, the S atoms as the neighbour in Pd_4S samples perturb the Pd electronic state, resulting in the relative increase of electron density of Pd, and consequence further decreases ethylene desorption from the Pd_4S surface, contributing to the enhanced selectivity of ethylene. More importantly, the catalytic performance of R350 sample maps on well to that previously reported for a nano-sized Pd_4S supported on carbon nanofibers.[49,50] This report therefore suggests that detailed characterisation of bulk phase materials can be useful for establishing links with analogous nano-sized particles which are challenging to characterise given their extremely small size.

Conclusions

The transformation of a palladium sulfide sample during thermal treatments has been assessed in detail. During reduction at temperatures of 150°C or higher, sulfur is lost to the gas phase, mainly as H_2S. Concurrently, the sample undergoes a phase change from a sulfur rich PdS phase to a sulfur lean Pd_4S phase (*via* the $Pd_{16}S_7$ phase as an intermediate). The extent to which this transformation occurs depends on temperature. Reduction at 250°C produces a material, which contains simultaneously these three phases with some Pd_4S phase is located at the surface. Reduction at 350°C almost exclusively converts the sample to the Pd_4S phase. Samples which contain a significant portion of the Pd_4S phase offer excellent activity and selectivity for acetylene hydrogenation even under competitive conditions. The selectivity is in part attributed to a site isolation effect brought about as a result of the crystal structure of Pd_4S, but also due to changes in adsorption desorption energetic brought about by changes to the Pd electronic state. No signs of deactivation or significant deposition of carbon were observed over Pd_4S sample after 50 h on stream.

Acknowledgements

References

[1] A. Borodziński, G. C. Bond, *Catal. Rev.* **2006**, *48*, 91–144.

[2] A. Borodziński, G. C. Bond, *Catal. Rev.* **2008**, *50*, 379-469.

[3] S. A. Nikolaev, I. L. N. Zanaveskin, V. V Smirnov, V. A. Averyanov, K. I. Zanaveskin, *Russ. Chem. Rev.* **2009**, *78*, 231–247.

[4] D. B. Tiedtke, T. T. P. Cheung, J. Leger, S. A. Zisman, J. J. Bergmeister and G. A. Delzer in: *13th Ethlyene Producers Conference*, **2001**, *10*, 1-21.

[5] S. Asplund, *J. Catal.* **1996**, *158*, 267.

[6] A. J. McCue, J. A. Anderson, Front. *Chem. Sci. Eng.* **2015**, *9*, 142–153.

[7] M. M. Johnson, D. W. Walker, G. P. Nowack, US Patent 4404124, 1983.

[8] D. Teschner, J. Borsodi, A. Wootsch, Z. Revay, M. Hävecker, A. Knop-Gericke, S. D. Jackson, R. Schlögl, *Science* **2008**, *320*, 86-89.

[9] M. García-Mota, B. Bridier, J. Pérez-Ramírez, N. López, *J. Catal.* **2010**, *273*, 92–102.

[10] B. Yang, R. Burch, C. Hardacre, G. Headdock, P. Hu, *J. Catal.* **2013**, *305*, 264–276.

[11] N. A. Khan, S. Shaikhutdinov, H. J. Freund, *Catal. Letters.* **2006**, *108*, 159–164.

[12] W. Ludwig, A. Savara, K. H. Dostert, S. Schauermann, *J. Catal.* **2011**, *284*, 148–156.

[13] F. Viñes, C. Loschen, F. Illas, K. M. Neyman, *J. Catal.* **2009**, *266*, 59-63.

[14] F. Studt, F. Abild-Pedersen, T. Bligaard, R. Z. Sorensen, C. H. Christensen, J. K. Norskov, *Science* **2008**, *320*, 1320-1322.

[15] Y. Liu, J. Zhao, Y. He, J. Feng, T. Wu, D. Li, *J. Catal.* **2017**, *348*, 135-145.

[16] Y. He, Y Liu, P. Yang, Y. Du, J. Feng, X. Cao, D. Li, *J. Catal.* **2015**, *330*, 61-70.

[17] Y. Zhang, W. Diao, J. R. Monnier, C. T. Williams, *Catal. Sci. Technol.* **2015**, *5*, 4123-4132.

[18] J. Feng, Y. Liu, M. Yin, Y. He, J. Zhao, J. Sun, D. Li, *J. Catal.* **2016**, *344*, 854-864.

[19] A. J. McCue, R. T. Baker, J. A. Anderson, *Faraday Discuss.* **2016**, *188*, 499-523.

[20] Y. N. Liu, J. T. Feng, Y. F. He, J. H. Sun, D. Q. Li, *Catal. Sci. & Technol.* **2015**, *5*, 1231-1240.

[21] A. J. McCue, C. J. McRitchie, A. M. Shepherd, J. A. Anderson, *J. Catal.* **2014**, *319*, 127–135.

[22] A. J. McCue, J. A. Anderson, *J. Catal.* **2015**, *329*, 538–546.

[23] A. J. McCue, A. Gibson, J. A. Anderson, *Chem. Eng. J.* **2016**, *285*, 384–391.

[24] A. J. McCue, A. M. Shepherd, J. A. Anderson, *Catal. Sci. Technol*. **2015**, *5*, 2880–2890.

[25] Q. Jin, Y. He, M. Miao, C. Guan, Y. Du, J. Feng, D. Li, *Appl. Catal. A: Gen.,* **2015**, *500*, 3-11.

[26] H. Zhou, X. Yang, L. Li, X. Liu, Y. Huang, X. Pan, A. Wang, T. Zhang, *ACS Catal.* **2016**, *6*, 1054-1061.

[27] G. Vilé, D. Albani, N. Nachtegaal, Z. Chen, D. Dontsova, M. Antonietti, N. López, J. Pérez-Ramírez, J., *Angew. Chem. Int. Ed.* **2015**, *54*, 11265-11269.

[28] J. Osswald, K. Kovnir, M. Armbrüster, R. Giedigkeit, R. E. Jentoft, U. Wild, Y. Grin, R. Schlögl, *J. Catal.,* **2008**, *258*, 219–227.

[29] M. Friedrich, S. A. Villaseca, L. Szentmiklósi, D. Teschner, M. Armbrüster, *Materials,* **2013**, *6*, 2958–2977.

[30] Q. Feng, S. Zhao, Y. Wang, J. Dong, W. Chen, D. He, D. Wang, J. Yang, Y. Zhu, H. Zhu, L. Gu, Z. Li, Y. Liu, R. Yu, J. Li, Y. Li, *J. Am. Chem. Soc.* **2017**, *139*, 7294-7301.

[31] L. Shao, W. Zhang, M. Armbrùster, D. Teschner, F. Girgsdies, B. Zhang, O. Timpe, M. Friedrich, R. R. Schlögl, D. Sheng Su, *Angew. Chem. Int. Ed.* **2011**, *50*, 10231-10235.

[32] G. Pei, X. Liu, A. Wang, A. F. Lee, M. A. Isaacs, L. Li, X. Pan, X. Yang, X. Wang, Z. Tai, K. Wilson, T. Zhang, *ACS Catal.* **2015**, *5*, 3717–3725.

[33] G. X. Pei, X. Y. Liu, X. Yang, L. Zhang, A. Wang, L. Li, H. Wang, X. Wang, T. Zhang, *ACS Catal.* **2017**, *7*, 1491-1500.

[34] G. Kyriakou, M. B. Boucher, A. D. Jewell, E. A. Lewis, T. J. Lawton, A. E. Baber, H. E. Tierney, M. Flytzani-Stephanopoulos, E. C. H. Sykes, *Science* **2012**, *335*, 1209-1212.

[35] H. L. Tierney, A. E. Baber, J. R. Kitchin, E. C. H. Sykes, *Phys. Rev. Lett.* **2009**, *103*, 246102-1-246102-4.

[36] M. B. Boucher, B. Zugic, G. Cladaras, J. Kammert, M. D. Marcinkowski, T. J. Lawton, E. C. H. Sykes, M. Flytzani-Stephanopoulos, *Phys. Chem. Chem. Phys.* **2013**, *15*, 12187-12196.

[37] F. M. McKenna, J. A. Anderson, *J. Catal.* **2011**, *281*, 231-240.

[38] F. M. McKenna, R. P. K. Wells, J. A. Anderson, *Chem. Comm.* **2011**, *47*, 2351-2353.

[39] F. M. McKenna, L. Mantarosie, R.P.K. Wells, C. Hardacre, J. A. Anderson, *Catal. Sci. Technol.* **2012**, *2*, 632-638.

[40] G. Vilé, N. Almora-Barrios, S. Mitchell, N. López, J. Pérez-Ramírez, *Chem. Eur. J.* **2014**, 20, 5926-5937.

[41] D. Albani, G. Vilé, S. Mitchell, P. T. Witte, N. Almora-Barrios, R. Verel, N. López, J. Pérez-Ramírez, *Catal. Sci. Technol.* **2016**, 6, 1621-1631.

[42] A. J. McCue, F. M. McKenna, J. Anderson, *Catal. Sci. Technol.* **2015**, 5, 2449-2459.

[43] G. Vilé, B. Bridier, J. Wichert, J. Pérez-Ramírez, *Angew. Chem. Int. Ed.* **2012**, *51*, 8620–8623.

[44] J. Carrasco, G. Vilé, D. Fernández-Torre, R. Pérez, J. Pérez-Ramírez, *J. Phys. Chem. C,* **2014**, 118, 5352-5360.

[45] G. Vilé, P. Dähler, J. Vecchietti, M. Baltanás, S. Collins, M. Calatayud, A. Bonivardi, J. Pérez-Ramírez, *J. Catal.* **2015**, 324, 69–78.

[46] D. Albani, M. Capdevilla-Cortada, G. Vilé, S. Mitchell, O. Martin, N. López, J. Pérez-Ramírez, *Angew. Chem.* **2017**, 56, 10755-10760.

[47] B. Bachiller-Baeza, A. Iglesias-Juez, E. Castillejos-López, A. Guerrero-Ruiz, M. Di Michiel, M. Fernández-García, I. Rodríguez-Ramos, *ACS Catal.* **2015**, 5, 5235–5241.

[48] B. Bachiller-Baeza, J. Peña-Bahamonde, E. Castillejos, A. Guerrero-Ruiz, I. Rodríguez-Ramos *Catal. Today,* **2015**, 249, 63-71.

[49] A. J. McCue, A. Guerrero-Ruiz, I. Rodríguez-Ramos, J. A. Anderson, *J. Catal.* **2016**, 340, 10-16.

[50] A. J. McCue, A. Guerrero-Ruiz, C. Ramirez-Barria, I. Rodríguez-Ramos, J. A. Anderson, *J. Catal.* **2017**, 355, 40-52.

[51] A. J. McCue, J. A. Anderson, *Catal. Sci. Technol.* **2014**, 4, 272–294.

[52] L. B. McCusker, R. B. Von Dreele, D. E. Cox, D. LoueÈr and P. Scardi, *J. Appl. Cryst.* **1999**, *32*, 36-50.

[53] Y. F. He, J. T. Feng, Y. Y. Du and D. Q. Li, ACS Catal., 2012,2, 1703.

[54] Y. F. He, L. L. Liang, Y. N. Liu, J. T. Feng, C. Ma and D. Q. Li,J. Catal., 2014, 309, 166.

[55] E. W. Shin, J. K. Kang, W. J. Kim, J. D. Park and S. H. Moon, *Appl. Catal., A,* **2002**, *223*, 161

[56] F. Grønvold, E. Røst, *Acta Chem. Scand.,* **1952**, *10*, 1620-1634.

[57] Q. Zhang, W. Xu, X. Li, D. Jiang, Y. Xiang, J. Wang, J. Cen, S. Romano, J. Ni, *Appl. Catal. A Gen.* **2015**, *497*, 17–21.

[58] V. V. Signh, U. Kumar, S. N. Tripathi, A. K. Singh, *Dalton Trans.* **2014**, *43*, 12555-12563.

[59] Feng Liu, Dominik Wechsler, Peng Zhang, Chemical Physics Letters 461 (2008) 254–259.

[60] P. Zhang and T. K. Sham, Appl. Phys. Lett., 4 (2002) 81.

[61] M. Fernández-García, Catal. Rev. Sci. Eng. 44 (2002) 59.

[62] M. Fernández-García, A. Iglesias-Juez, A. Martínez-Arias, A. B. Hungría, J. A. Anderson, J. C. Conesa, and J. Soria, J. Catal. 221 (2004) 594–600

[63] A. Iglesias-Juez, A. Martínez-Arias, M. A. Newton, S. G. Fiddy and M. Fernández-García, Chem. Commun., **2005**, 4092–4094.

[64] H. Murayama, N. Ichikuni, Y. Negishi, T. Nagata, T. Tsukuda, *Chem. Phys. Lett.* **2003**, *376*, 26-32.

[65] F. Grønvold, E. Røst, *Acta Cryst.* **1962***, 15*, 11-13.

[66] J. B. Miller, D. R. Alfonso, B. H. Howard, C. P. O-Brien, B. D. Morreale, J*. Phys. Chem. C* **2009***, 119*, 18800-18806.

[67] C. Ma, Y. Y. Du, J. T. Feng, X. Z. Cao, J. Yang, D. Q. Li, *J. Catal.* **2014**, 317, 263–271.

[68] Y. Azizi, C. Petit, V. Pitchon, *J. Catal.* **2008**, *256*, 338-344.

[69] B. Radha, G. U. Kulkarni, *Adv. Funct. Mater.* **2010**, 20, 879−884.

[70] C. N. Rao, K. K. Rao, *Ca. J. Phys.* **1964**, *42*, 1336-1342..

[71] Y. Luo, S. A. Villaseca, M. Friedrich, D. Teschner, A. Knop-Gericke, M. Armbrùster, *J. Catal.* **2016**, *338*, 265-272.

[72] W. J. Kim, I. Y. Ahn, J. H. Lee and S. H. Moon, *Catal. Commun.,* **2012**, 24, 52.

[73] E. Kim, E. W. Shin, C. W. Bark, I. Chang, W. J. Yoo and W. J. Kim, *Appl. Catal., A,* **2014**, 471, 80